Nanoparticle Effects on the Morphology and Mechanical Properties of Polypropylene Spunbond Webs

Raghavendra R. Hegde, Gajanan S. Bhat

Department of Materials Science and Engineering, University of Tennessee, Knoxville, Tennessee 37996-2200

Received 1 September 2009; accepted 19 February 2010
DOI 10.1002/app.32304
Published online 9 July 2010 in Wiley InterScience (www.interscience.wiley.com).

ABSTRACT: We report morphology and mechanical properties of natural nanoclay incorporated spunbond polypropylene composite webs. Nanocomposite spunbond webs were produced with up to 5 wt % natural nanoclay additives on Reicofil®-2 spunbond line. Influence of nanoclay on the resin rheological properties, processibility, and mechanical properties of webs were studied. Wide angle X-ray diffraction and transmission electron microscopy analysis were used to investigate the nanocomposite morphology. Intercalated and flocculated morphology was observed for all the concentrates and for all the spunbond fiber webs. The microstructure and polymer morphology in the presence of additives was characterized using a polarized optical microscope. At higher percentage, excess clay platelets were excluded out of the spherulite boundaries. About 20–30% increase in tear strength was observed for webs with up to 2 wt % nanoclay additives. Compared with the control polypropylene spunbond web, nanoclay reinforced samples showed better dimensional stability. Different failure mode was observed for spunbond webs with additives. Spunbond webs with even as low as 1 wt % clay retain their morphology and integrity in bond point after thermal bonding. Nanoclay incorporated spunbond webs showed significant improvements in the stiffness. © 2010 Wiley Periodicals, Inc. J Appl Polym Sci 118: 3141–3155, 2010

Key words: additives; nanotechnology; nanocomposites; polypropylene; structure-property relations

INTRODUCTION

In recent years, nanoclay has gained enormous industrial and academic research interest because of its potential in improving the thermal and mechanical properties of polymer matrix in which it is incorporated.[1] In addition to its property benefits, its ability to be processed using existing melt processing and incorporation in the end products like fibers,[2] films, nonwoven webs,[3] and molded parts is very beneficial.[1,4,5]

One of the challenges of the nanoclay additives is the difficulties associated in uniformly dispersing the additives in the matrix.[1] Many studies have attempted to modify the clay additives to minimize the agglomeration.[6–11] Based on the extent of exfoliation, there are three known morphologies of polymer nanoclay composites. Phase separated morphology is similar to conventional micro composites where, additives form micron size agglomerates. As far as intercalated morphology, few polymer chains are intercalated between the clay platelets such that interlayer spacing is expanded, but layers still retain well defined spatial configuration. With regard to intercalated morphology, the peak corresponding to the clay in wide angle X-ray diffraction (WAXD) scan increases or decreases depending on extent of chain intercalation. Finally, for exfoliated morphology, the clay platelets are completely separated and individual layers are well dispersed in the matrix. In exfoliated morphology, interlayer distance and platelet length depend on the type of matrix and processing conditions used to manufacture the product.[1,3]

Extent of dispersion of clay in the end product also depends on the type of matrix. As far as polyamides it is relatively easy to disperse clay additives in matrix because of their polar nature.[1] Zhang et al. described polypropylene (PP) system as immiscible while polyethylene (PE) matrix is likely to give intercalated morphology. With regard to polypropylene (PP), because of its apolar nature, it is difficult to disperse the additives in the matrix or resultant product, despite using compatibilizers and dispersion agents. Most of the earlier literatures report intercalated and flocculated morphology in PP which is essentially a mixture of intercalated and flocculated morphology.[12]

To achieve a reasonable extent of intercalation of the clay in polyolefin requires the inclusion of a compatibilizer at the clay–polymer interface.[8–11] Polypropylene-*grafted*-maleic anhydride (PP-*g*-MA) is one of the widely investigated compatibilizers in synthesis of PP-nanoclay composites.[3,13,14] In this research, linear low-density polyethylene (LLDPE) based maleated wax was used as

Additional Supporting Information may be found in the online version of this article.

Correspondence to: G. S. Bhat (gbhat@utk.edu) or R. R. Hegde (rhegde@utk.edu).

a compatibilizer between the PP and Closite Na^+. Details of possible interaction between the clay platelet, PP chain, and compatibilizers are reported in previous literatures.[3,13–17]

Spunbonding is a one step integrated fabric production method consisting of filament spinning, formation of random web and thermal bonding. The fabrics are produced by depositing extruded, spun filaments onto a collecting belt in a uniform random manner followed by bonding the fibers.[18] The spunbond (SB) fabrics are used for wide range of applications ranging of from disposable medical/hygiene products to automotive/civil, engineering products.

In our previous studies, we investigated properties of SB webs with natural (Closite Na^+) and organo-modified (Cloisite 15A) nanoclay additives.[3] Improvements in mechanical properties of PP SB webs were observed by inclusion of 1 wt % nanoclay. Compared with natural nanoclay, organo modified clay platelets gave slightly better dispersion and property benefits. Inclusion of additives improved fiber strength to the order of 15 to 75%. Observed increase in tensile strength and modulus of the webs was 10 to 20%, both in the machine and cross directions. Similarly, bending length or stiffness of the fabric increased by 10 to 25%. Substantial increase in burst strength, to the order of 20 to 80%, was observed.[3] However, one of the disadvantages of organo-modified nanoclay additives is that it undergoes thermal degradation during melt processing. Thermal degradation leads to loss of surfactants from clay platelets. The extent of degradation increases as the processing temperature becomes higher and the rate of surfactant loss increases beyond 200°C. Shah and Paul reported greater mass loss of surfactant during melt processing of nanocomposites compared with mass loss calculated by thermo gravimetric analysis (TGA) of organoclays.[19] Also, the SB webs, meltblown webs, and carded webs with functionalized MnO nanoclay additives have been produced and investigated for their functional properties. The webs had effective odor removal properties.[20]

The nanocomposite morphology within the spunbond fiber webs has not been investigated before. Distribution and extent of polymer chain intercalation within clay platelets in SB fiber webs is unknown. In this research, influence of the additives on the processibility, microstructure, morphology, and mechanical property of nanocomposite fibers and nonwoven webs are investigated. The results obtained are more relevant to the nonwoven industry.

EXPERIMENTAL

Materials and method

All the PP resin samples were prepared with different percentage of natural nanoclay additive Closite Na^+ purchased from Southern Clay Products of Gonzales, Texas. The PP was compounded with 1–5 wt % of nanoclay additive at Techmer PM, Clinton, TN. The PP, maleated wax and Closite Na^+ were melt compounded in a counter rotating twin screw extruder (L/D = 28 : 1 mm). The extrusion zone temperatures were in the range of 204 to 210°C to produce concentrates containing clay wt % as shown in Table I. Each of these concentrates contained 5 wt % maleated wax produced by Honeywell (product AC573) as a dispersion agent.

TABLE I
Polypropylene with Different Additives Used for the Spunbond Trial

Sample	Dispersion aid	Matrix
Control PP		PP
1% clay	5% maleated wax	94% PP
2% clay	5% maleated wax	93% PP
5% nanoclay	5% maleated wax	90% PP
5% clay	5% maleated wax	60% maleated PP + 30% PP

Spunbond (SB) fabrics were produced from polymer concentrates (listed in Table I) on Reicofil®-2 spunbonding line at the University of Tennessee. Schematic of Reicofil®-2 spunbond line based on melt spinning technique is shown in Figure 1. Polymer concentrates (shown in Table I) are fed in to the hopper (1) by vacuum suction. Pellets are melted by the hot walls of barrel (2) and pushed forward by the flight of screw. Viscous polymer melt then passes through the screen pack, which filters any contaminants in the melt. Pressurized molten polymer is conveyed to a metering pump that regulates the quantity of melt delivered to die assembly for spinning.[21]

Die block assembly consists of feed distribution and spinneret. Feed distribution manages the uniform distribution of melt all the way through the width of the die block.[22] The polymer melt is forced by spin pumps (3) through a special spinneret (4) which consists of single metal block with thousands of very precisely drilled orifice. The primary blow ducts (6), located below the spinneret block, continuously cool the filaments and the secondary blow ducts (7), located below the primary blow ducts, continuously supply the auxiliary room temperature air. Over the line's entire working width, ventilator generated under pressure sucks the filaments and mixed air down from spinnerets and cooling chambers (5). The continuous filaments are sucked through a venturi (high velocity, low pressure zone) to a distributing chamber (8), which affects the entanglement of the filaments. Finally, the entangled filaments are deposited as a random web on a moving sieve belt (10).

Spun fiber samples from the collector screen at point (11) and the SB web samples wound on the winding unit (14) were collected for characterization. Target basis weight for all the samples was 30 gsm (grams/square meter). Spunbond run was quite

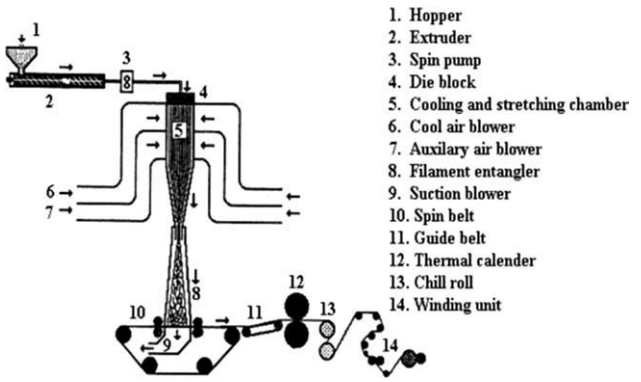

Figure 1 Schematic of spunbond line.[18]

normal for all formulations except for 5 wt % nanoclay in the maleated PP matrix (60% maleated PP + 30% PP), for which melt filter at the end of the extruder stopped and could not be processed further. All the compositions were processed under similar conditions as shown in Table II.

TESTING AND CHARACTERIZATION

Rheological characterization

The rheological properties of nanoclay incorporated polypropylene concentrates, such as viscosity and shear rate at different temperatures were analyzed using the Advanced Rheometric Expansion System (ARES) 2000 capillary rheometer. Tests were carried out at 240°C at shear rates ranging from 10 to 10,000 sec^{-1}. Capillary tube with length to diameter ratio of 25/1 mm was used.

Wide angle X-ray diffraction (WAXD)

Wide angle X-ray diffraction is ideal for analysis of nanoclay incorporated samples because of the presence of periodic structure in neat clay as well as in the clay reinforced nanocomposites.[14] In this work, WAXD scans of the chopped fiber samples were carried out in reflection mode to determine change in crystallinity wt %, and clay dispersion. Samples were scanned in the 2θ range of 2 to 40° and step size of 0.02 at 1 sec for each step. Crystal size (t) was calculated using the Scherrer equation [eq. (1)], from the measured full width half maximum (FWHM) intensity of reflection peaks in the equatorial scans.[23]

$$t = \frac{0.9\lambda}{B\cos\theta} \tag{1}$$

where λ is the wavelength (1.542 A°) and B the measured FWHM intensity of (110) reflection peaks. WAXD analyses were carried out using the Phillips X Pert Pro X-ray diffraction system with CuKα radiation (45 kV, 40 mA) of wavelength 1.542 A°.

Transmission electron microscopy (TEM)

For the nonwoven webs, a special technique was used to prepare samples for TEM. (Schematic of TEM sample sectioning is shown in Supporting Information Fig. S1). Spunbond webs were doped within the epoxy block and ultrathin sections (50 to 70 nm thick) were microtomed using RMC Power tome CRX microtome equipped with diamond knife. Specimen temperature was –100°C and knife temperature was set to –103°C. Sections were mounted on standard 400 mesh Cu grids and TEM images were taken using the Hitachi H-800 Electron Microscope operated at 75 kV.

Differential scanning calorimetry (DSC)

Thermal analysis was carried out using the Mettler Toledo DSC 822e. Fiber samples were scanned in the temperature range from 25°C to 205°C at heating and cooling rates of 10°C per minute in the N_2 atmosphere. Percentage of crystallinity, X_c%, of nanoclay incorporated samples were calculated from enthalpies of crystallization using eq. (2),

$$X_c\% = \frac{\Delta H}{(1-\varphi)\Delta H_{100\%}} \times 100 \tag{2}$$

where, ΔH is the measured heat of fusion of the sample, $\Delta H_{100\%}$ the heat of fusion of the 100% crystalline polypropylene which is taken as 190 J/g and φ is the weight fraction of Closite Na^+ nanoclay additive.[24]

Nonwoven testing

Samples of spun fiber and spunbond fabrics were conditioned for 24 h in a conditioned laboratory according to ASTM D1776 (standard laboratory conditions of 65 ± 2% RH (relative humidity) and temperature of 21± 1°C). After conditioning samples were, analyzed for physical properties and structure according to ASTM D1117-97 - Standard Test Methods for Nonwoven fabrics.[25]

TABLE II
Spunbond Run Conditions

Melt temperature	240°C
Through put	0.43 g/hole/min
Extruder pressure	12.4 mPa
Spin pump speed	9.3 rpm
Air suction/Fiber suction Speed	1490 rpm
Calendering temperature	145 °C
Belt speed	25 m/min

Thicknesses of fabric samples were measured using the TMI thickness tester as per ASTM D5729-97. Bending length was estimated using the cantilever bending test method as per ASTM D5732-95. The rectangular fabric strip of 37.5 mm × 2.5 mm sample was placed on the horizontal platform with the engraved scale and slid at constant rate along with template. Length was noted down when the sample bends under its own weight and makes an angle of 41.5° with the horizontal platform. Each sample was tested four times on both sides (top, bottom) and by turning (right, left). Extent of color change due to additives was determined using a Miniscan Hunter Colorimeter. Tear strength was measured as per ASTM D5734-95 using the Elmendorf tear tester. Burst strength was tested using the B F Perkins, Mullen burst strength tester as per ASTM D3786-87. Tensile properties were determined using the United tensile tester as per ASTM D3822-07. Sample dimension of 25 mm width and 75 mm gage length were used for tensile test and stretched to break at a uniform strain rate of 0.0034 cm/min.

Dimensional stability of nonwoven fabrics was measured as per ASTM D2724-87. Washed samples were analyzed for appearance and dimensional shrinkage using eq. (3),

$$\text{Shrinkage}_c\% = \frac{(A - B)}{A} \times 100 \quad (3)$$

where, A-average original length between marks, and B-average final length between marks.[25]

Statistical analysis

To calculate the statistical significance for difference in mechanical properties for different sample with nanoclay additives compared with control PP web, the unpaired two-tailed Student's t test was performed. The Michelin guide scale is used to indicate statistical significance of difference between control PP and web samples with clay additives. The P values of less than 0.05 were considered significant and the difference in results is expressed as figure legends asterisk (*). For example, if P value of less than 0.05 are marked with one asterisk (*). The P value $\leq$ 0.05 (*), P value $\leq$ 0.01 (**), P value $\leq$ 0.001 (***) were considered significant. P value greater than 0.05 were considered not significant (expressed as legend ns).

Polarized light microscopy (PLM) analysis of spherulite

Extent of inclusion and exclusion of additives from the matrix was compared using the spherulite microstructure analysis. Small sections of PP pellets were kept in between the glass plate and the cover slide. Samples were isothermally melted using METTLER FP82HT hot stage controlled by FP90 Processor at 205°C, zero pressure and kept in molten state for 10 min to ensure complete melting.

The glass slide is immediately switched to second hot stage maintained at room temperature and allowed to cool for 30 min. Average thickness of the crystallized film was less than 200 μm. Spherulite images were analyzed using Olympus BX51 polarized optical microscope. Maximum diameter of spherulite for each sample was determined for average of $n = 30$ spherulite measurements. From the average maximum attainable diameter values, nucleation density of spherulite N was calculated using eq. (4),

$$N = \left(\frac{3}{4}\pi\right)(D_m/2)^{-3} \quad (4)$$

where, D_m is the maximum attainable diameter of spherulite before impingement.[26]

Birefringence

The optical retardation of spunbond fibers (fibers in the SB web) was determined using Olympus BX51 polarized optical microscope equipped with a 20X analyzer eyepiece and tilting compensator B. From the optical retardation (R) birefringence (Δn) is estimated using eq. (5),

$$\Delta n = \frac{R}{t} \quad (5)$$

Scanning electron microscopy

Scanning Electron Microscopy (SEM) images of the SB web surface and web failure structure were taken using the Leo 1215 Field emission gun. The samples were coated for 10 s using the SPI sputter coater. Image magnifications were in the range of ×100 to ×1700.

To count the area of interspherulite region between the different concentrates, Image J and Image Pro Plus software's were used. The example of an SEM micrograph of PP with 1 wt % clay analyzed using the Image pro plus count size tool is shown in Supporting Information Figure S2.

Energy dispersive spectrometers (EDS)

The Oxford Pentafet EDS system was used along with SEM to identify the elimental composition in the small area of interest like: failure spots of nanocomposite and of interspherulite regions. ZAF Quantitative method, ZAF (3 iterations) with the system resolution of 127 eV and running Link ISIS software were used for data analysis.

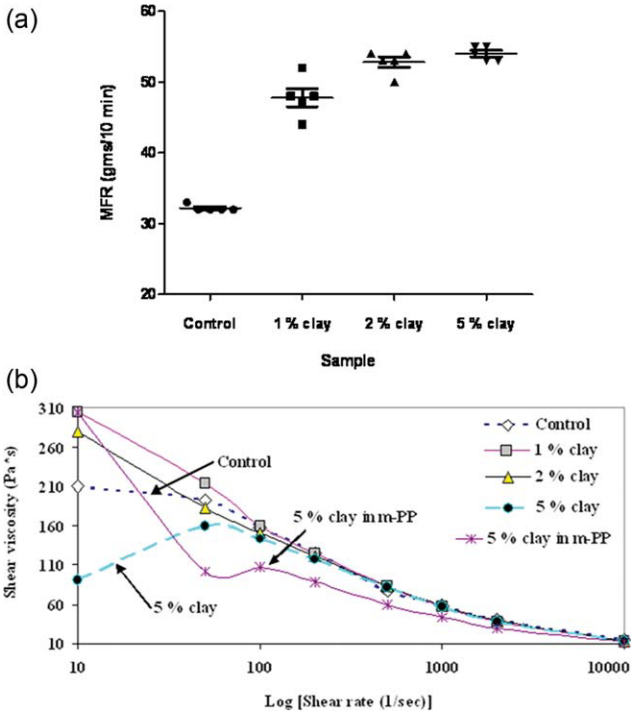

Figure 2 (a) Results of melt flow rate (MFR), (b) Capillary rheometry results of PP concentrates. [Color figure can be viewed in the online issue, which is available at www.interscience.wiley.com.]

RESULTS

Rheology of concentrates with clay

Results of melt flow rate (MFR) are summarized in Figure 2(a). Concentrates with clay additive had slightly higher melt flow rate (MFR), which is beneficial from processing point of view. Variation in shear viscosity at different shear rates for resins with different percentage of clay is shown in Figure 2(b). Overall, shear viscosity for resin with clay in low shear range of 100 sec^{-1} is higher than that of control. At higher shear rate of beyond 100 sec^{-1} samples with clay additive show shear thinning behavior. Difference in shear viscosity is due to difference in dispersion of nanoclay additives in each of these concentrates.

Shear viscosity decreases and levels off at extremely high shear rates of the order of 10,000 sec^{-1}. Higher shear viscosity for resin with clay in low shear range of 100 sec^{-1} is due to the hindrance caused by the nano additive particles. Sample with 5% clay shows thixotropic behavior of increasing shear viscosity at lower shear rates. However, the concentrate with 5% clay in maleated polypropylene (m-PP) had the opposite effect at low initial shear rates and a slight increase in shear viscosity at shear rate of 100 sec^{-1} and final reduction. This 5% concentrate could not be processed because of high viscosity, pressure rise and filter clogging.

The increase in shear viscosity is due to formation of loop like conformations between polypropylene chains, maleated polypropylene and clay platelets. At higher shear rates ($\sim$ 10,000 sec^{-1}), shear viscosity decreases and levels off due to the disentanglement of nanoclay platelets and the polymer chains.[27] Critical shear rate is lower for PP with nanoclay additives. The shear thinning behavior at higher shear rates is due to the alignment of clay platelets in spinneret orifice parallel to the applied load.[28,29] Results of MFR are in accord with the shear viscosity results.

Structure and morphology of nanocomposite sb web

WAXD scans of different SB fabric samples and natural nanoclay are shown in Figure 3. The peak positions and respective reflection indices are labeled as shown in Figure 3. Reflection indices are similar for all the samples except for 5 wt % clay in maleated PP with respect to (040) peak. The decrease in (040) peak for sample with 5 wt % clay is due to slightly

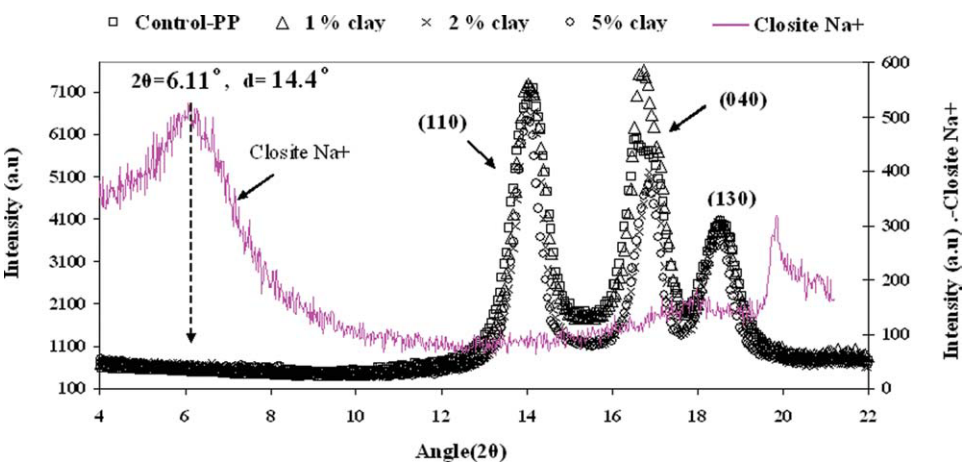

Figure 3 WAXD scans of spun fiber samples. [Color figure can be viewed in the online issue, which is available at www.interscience.wiley.com.]

TABLE III
Results of Fiber Crystallinity (%) and Crystal Size (A°)

Sample ID	Crystal size (A°)	Crystallinity wt %	
		WAXD	DSC
Control	137	52	54
1% clay	136	49	50
2% clay	160	51	51
5% clay	148	50	50

larger size clay tactoids which hinder the growth in (040) direction.[13]

Results of web crystallinity (%) and crystal size (A°) are shown in Table III. The observed crystal size differences are small with no specific trends. However, for sample with clay, apparent slight increase in crystal size might be due to segregation of clay platelets at the spherulite boundary as reported in earlier research for polypropylene/clay hybrids.[26] Crystallinity wt % was slightly lower for webs with additives, which is due to the hindrance to the polymer chain diffusion, and crystallization by dispersed clay platelets. Although the observed differences in values are not big here, the changes in crystallinity and crystal size values follow the trend as explained on the crystal growth studies with clay in our article.[3]

WAXD scans of webs do not show any peaks corresponding to natural nanoclay (around 2θ of 6.11°), which is due to very high levels of extrusion involved during spunbond process and delamination of the clay platelets.[30] Hence, TEM was used to get information about the presence and extent of dispersion of clay within web samples.[3]

TEM image of neat nanoclay is shown in Figure 4(a). Dark shady lines (50 nm) in the image represent the multiple layers of clay platelets, each of thickness less than 10 Å. TEM micrographs of concentrates with 1, 2, and 5 wt % clay, which were used to produce the SB web samples are shown in Figure 4(b,c,d). Micrographs revealed intercalated and flocculated morphology for all the concentrates. Each of the clay stacks has significant chain intercalation. Similar dispersion and morphology has been reported for PP/clay nanocomposites in earlier literatures.[1,31]

TEM micrographs of SB web samples are shown in Figures 5, 6, and 7. Micrographs contain section of fiber within epoxy matrix. Dark shady lines within the fiber represent nanoclay stacks. Good dispersion was observed for concentrates with 1 and 2 wt % clay in the polypropylene matrix (shown in Figs. 5 and 6). Mixtures of intercalated and exfoliated morphology were observed in the case of sample with 5 wt % clay (shown in Fig. 7).

Presence of clay stacks near the fiber surface, or protrusion of clay stacks from the fiber surface

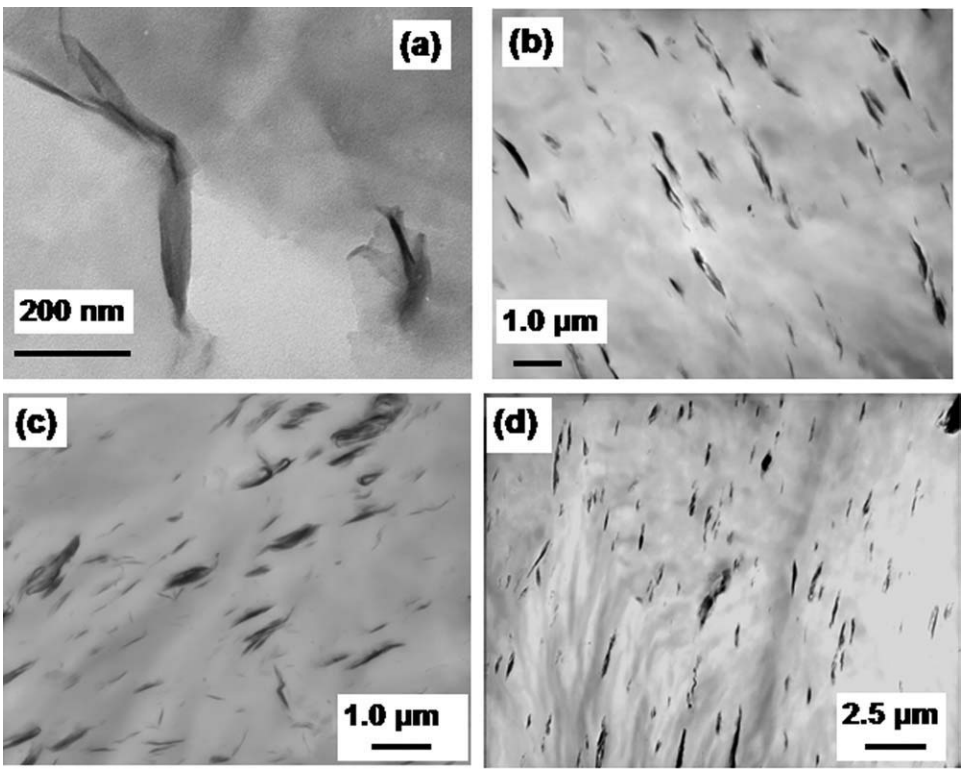

Figure 4 TEM micrographs of concentrates (a) neat clay Closite Na^+, (b) with 1 wt % clay, (c) with 2 wt % clay, and (d) with 5 wt % clay.

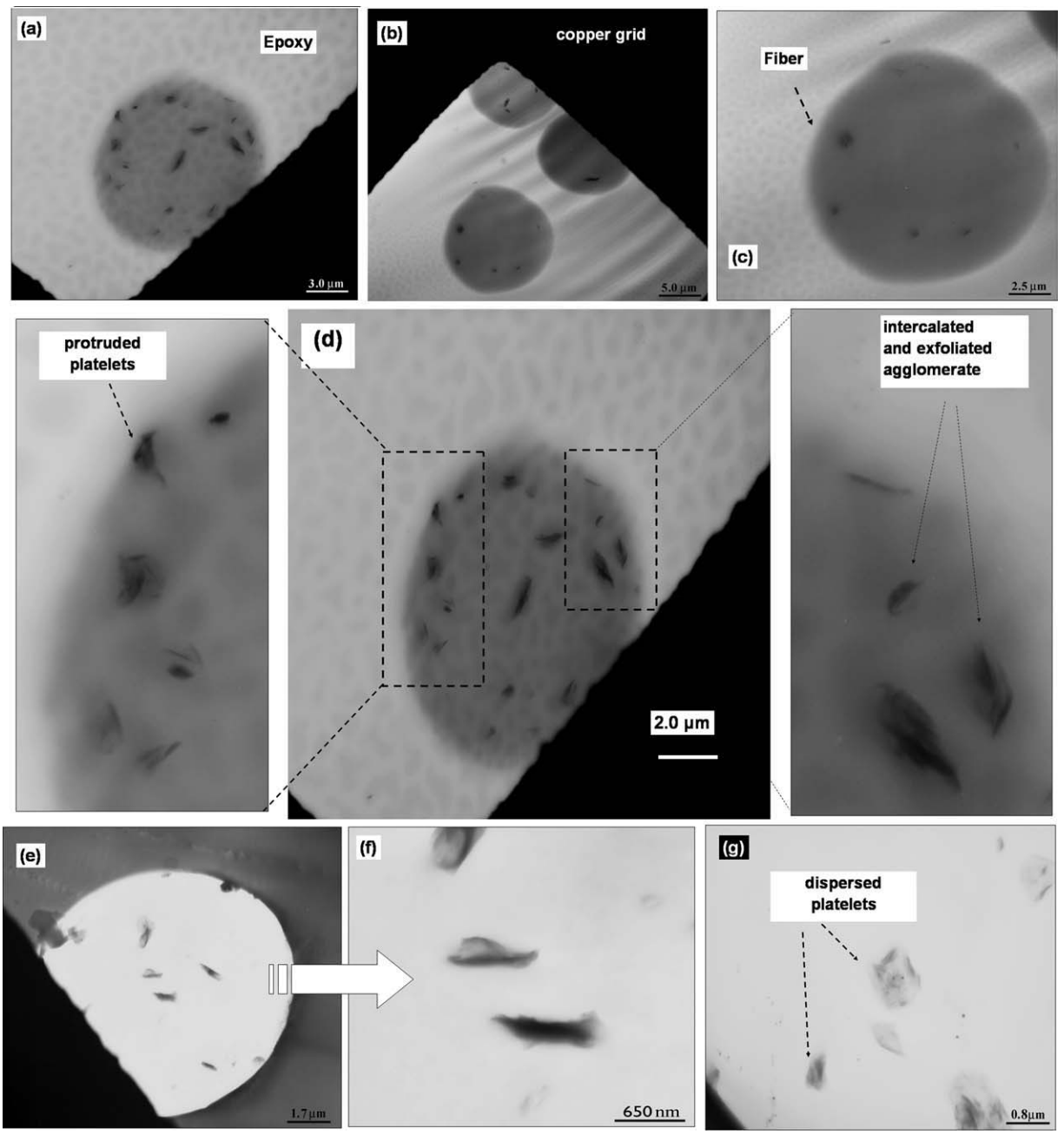

Figure 5 (a), (b), (c) TEM micrographs of concentrate with 1 wt % clay, (d) magnified micrograph showing particles at high magnification, (e) micrograph of fiber embedded in epoxy, (f) magnified micrograph at center of fiber with intercalated tactoids, and (g) dispersed platelets.

leads to significant difference in fiber surface topology as shown in Figure 7(a). Micrographs also reveal difference in the clay stack distribution along the fiber cross-section. Clay stacks near the fiber diameter are smaller fragments and oriented along the spinning direction, but the additives at center portion of the fiber are larger and randomly oriented as shown in Figure 7(b). Also, the particles near fiber surface have higher polymer chain intercalation compared with ones at the center as shown in Figure 7(c). This difference in the additive distribution is due to the "wall effect," an effect which leads to reduction in concentration of suspension adjacent to the solid wall of flow channel. Higher shear rate is created near the fiber surface and the additive particles migrate to the center. Effect is more prominent in the case of sample with 5 wt % additives as shown in Figure 7(a,d). Slightly higher number of clay stacks was observed in micrographs with 5 wt % additives, but the stacks had significant chain intercalation as shown in Figure 7(e,f).

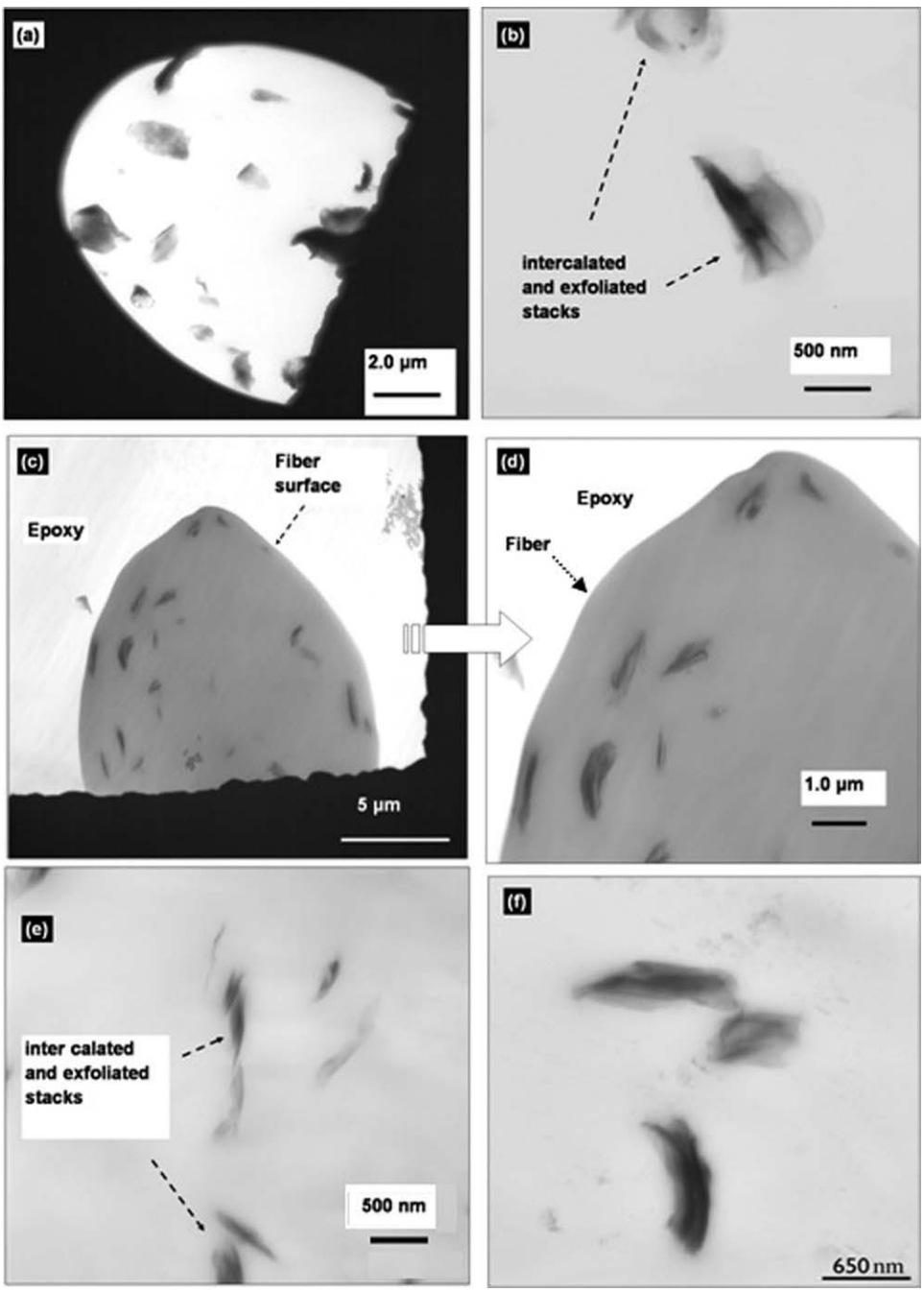

Figure 6 (a) TEM micrograph of film with 2 wt % clay, (b) magnified micrograph showing particles at high magnification, (c) micrograph of fiber with 2 wt % clay embedded in epoxy, (d) magnified micrograph, (e) and (f) micrograph at higher magnification show significant polymer chain intercalation.

Comparing the TEM micrographs of PP concentrates (shown in Fig. 4) and SB webs (Figs. 5, 6, and 7) it is clearly evident that clay stack morphology observed in the PP concentrates is also present in the SB webs. TEM micrographs convey two important facts;

i. Difficulty in getting exfoliation for of PP matrix, and
ii. Need for better dispersion in the concentrates to get higher dispersion in the fiber based nanocomposite end product.

Properties of nanoclay incorporated spunbond web

The properties of SB webs are summarized in Table IV. The SB web sample basis weight was 30 gsm (grams/square meter); fiber diameter was 15 μ and

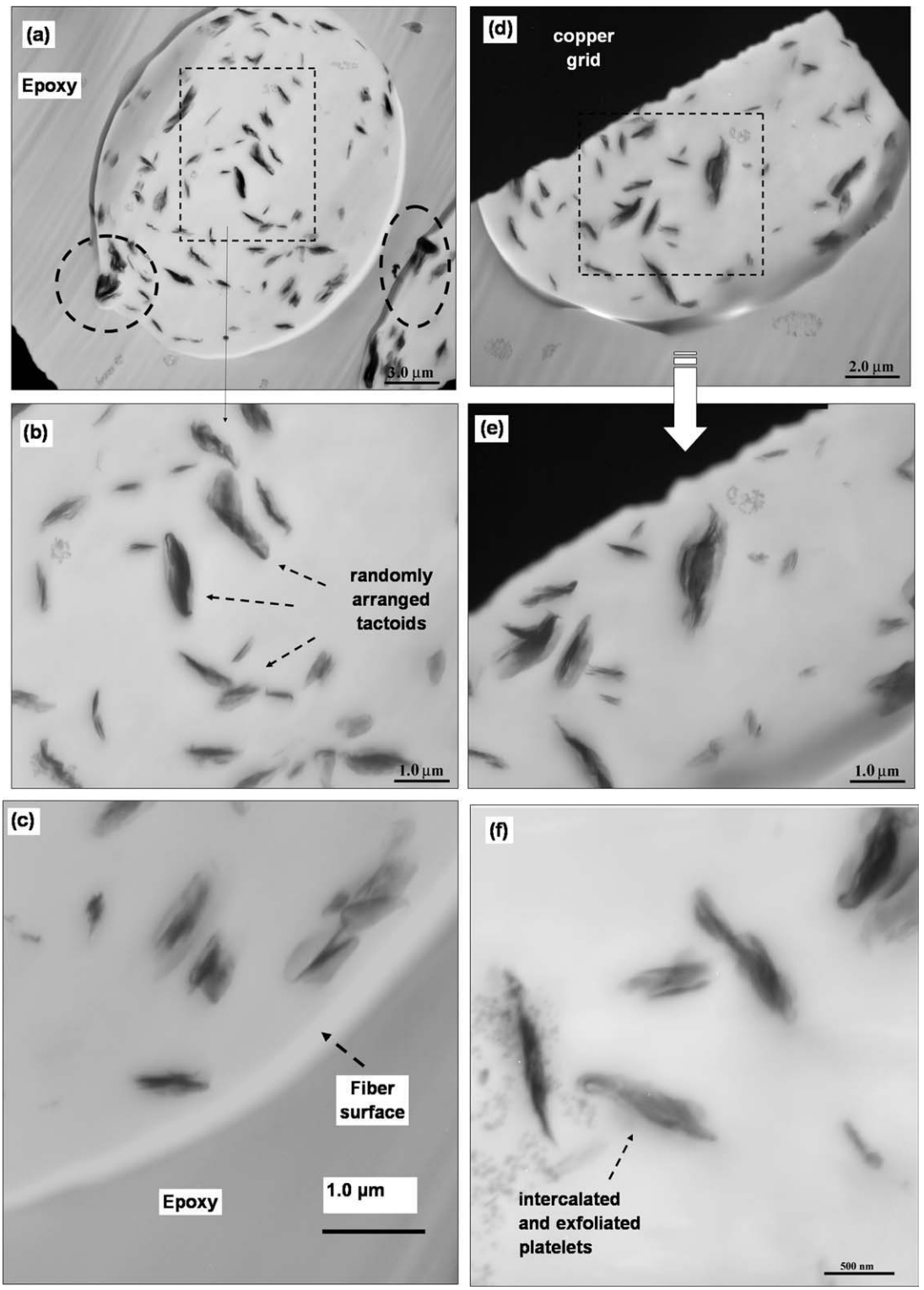

Figure 7 TEM micrographs of sample with 5 wt % clay (a) two fiber micrographs at their surface show protruding clay agglomerate, (b) randomly oriented particles at center, (c) platelets near the fiber surface with slightly higher intercalation, (e) and (f) tactoids with significant chain intercalation.

the web thickness was in the range of 300 microns (Table IV). Sample with 5 wt % clay had high b value (yellowness) which is due to the maleated wax.

Machine direction (MD) tensile strength results are summarized in Figure 8(a,b). Statistical significance of the differences is expressed using figure legends (detailed explanation is included in

TABLE IV
Properties of Spunbond Web with Nanoclay Additives

Sample	Weight (g)	Thickness (mm)	Fiber diameter (μ)	Birefringence (Δn)	Yellowness (b)
Control	30	0.3	15.8	0.015	0.7
1% clay	30	0.3	15.3	0.019	2.6
2% clay	30	0.3	16.7	0.017	3.5
5% clay	30	0.3	18.9	0.013	5.2

Statistical Analysis section). Even though MD tensile strength shows decreasing trend with additives, drop in strength is not significant for 1 and 2 wt %. However, at higher add on level of 5% clay, the strength drop was significant. The MD tensile strength test involves axial strain on the sample. During the tensile testing strength improvement in nanocomposite requires efficient load transfer between clay platelet and matrix. Intercalated and flocculated morphology has higher probability of

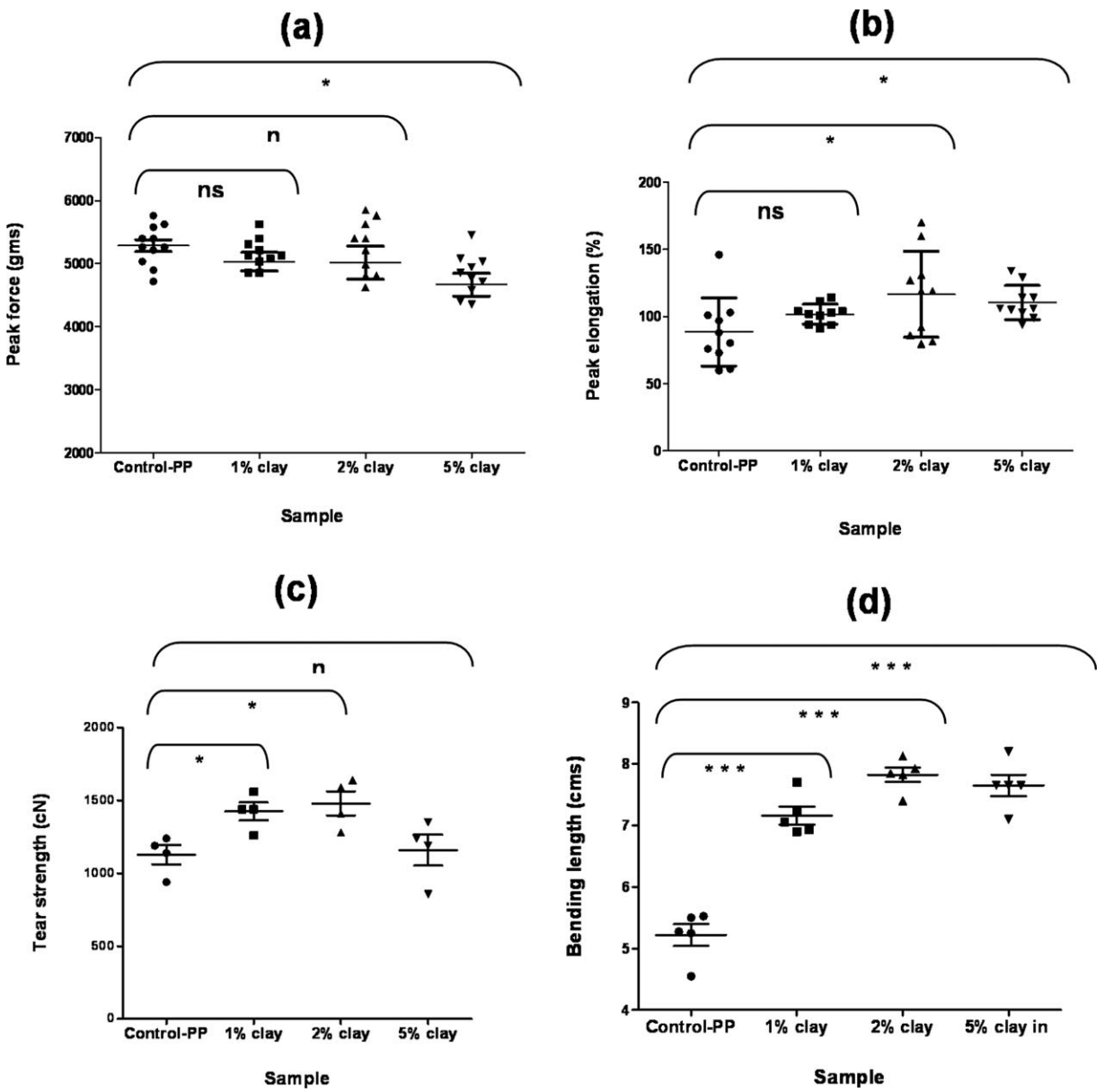

Figure 8 (a) Tensile strength in machine direction (MD), (b) Elongation properties of web samples, (c) tear strength in cross direction (CD) and (d) MD direction bending length of spunbond webs along machine direction (MD). Statistical significance: P value ≤ 0.05 (*), P value ≤ 0.01 (**), P value ≤ 0.001 (***) were considered significant. The P value > 0.05 are considered not significant (expressed as legend ns).

interparticle interaction which prevents efficient load transfer between platelet and matrix. Web elongation showed slightly increasing trend till 2 wt % clay loading as shown in Figure 8(b). Results of nonwoven web tear strength are shown in Figure 8(c). About 25 to 30% increase in cross direction (CD) tear strength was observed for 1 to 2 wt % clay loading. Beyond 2 wt % clay loading, tear strength shows decreasing trend, but the difference is not significant. Results of nonwoven web stiffness are shown in Figure 8(d). Nonwoven web stiffness significantly increased for all the SB samples with additives. However, increasing trend is observed only up to 2 wt % additives. Increase in additive wt% beyond 2 wt % did not bring any stiffness improvements. Only the web stiffness [shown in Fig. 8(d)] showed statistically significant improvement which is due to the presence of high modulus (in range of 20–400 Gpa[32]) clay stacks.

Variation in SB web shrinkage along machine direction (MD) and cross direction (CD) is shown in Figure 9(a,b). Overall web shrinkage showed decreasing trend for sample with nanoclay additives. The statistical significance of the difference compared to control is represented by the figure legends (*). Significant difference in SB web shrinkage is observed only along cross direction (CD) as shown in 9(b). During shrinkage, molecular networks tend to relieve from axial internal stress frozen in the fiber during processing and assume thermodynamically stable random state from supplied external heat.[33] Lower shrinkage observed in the case of nanoclay incorporated SB webs is due to reinforcement in the molecular network as shown in Figure 9(c).

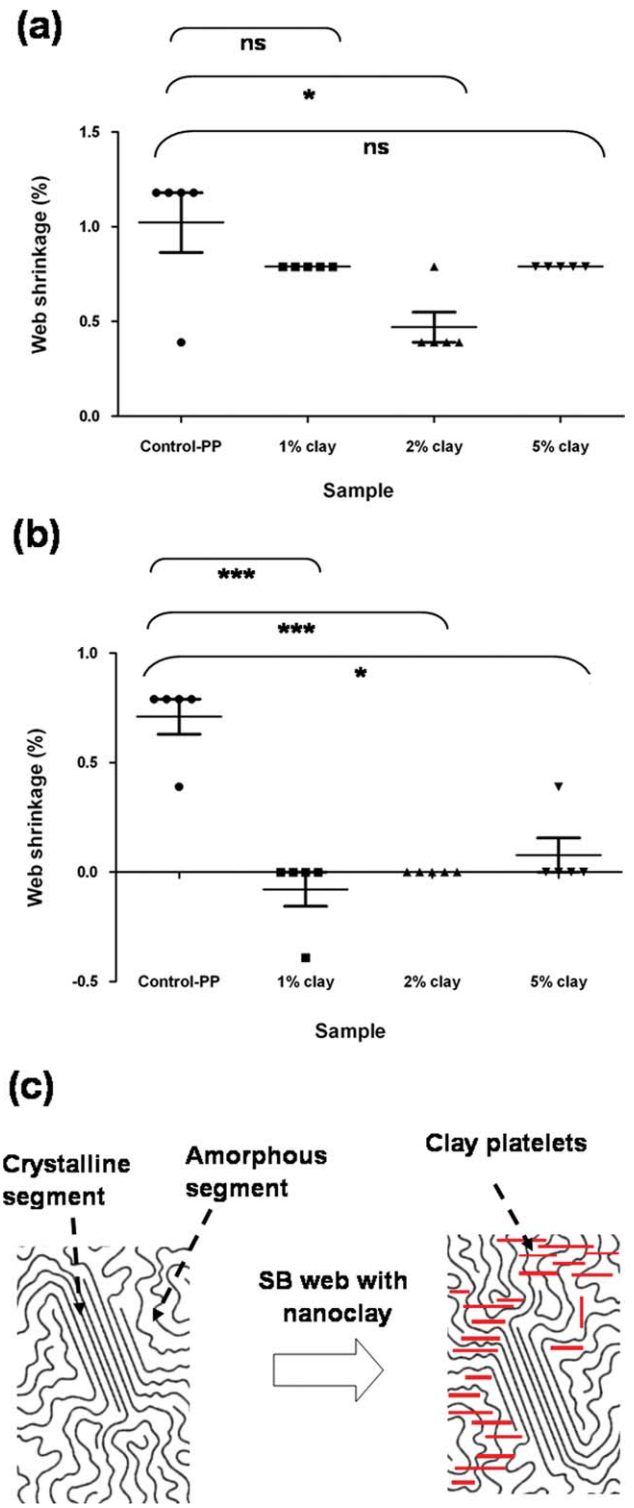

Figure 9 SB web shrinkage along (a) machine direction (MD), (b) cross direction (CD), (c) reinforcement of molecular network. [Color figure can be viewed in the online issue, which is available at www.interscience.wiley.com.]

Microscopy

The thermal bonding conditions were same for all the webs and bonding temperature was not optimized. However, careful examination of several bond points revealed difference in bond point, failure mode, and surface microstructure. SEM micrographs of bond point of control PP SB web and web with 1 wt % clay are shown in Figure 10(a,b). Fibers with even as low as 1 wt % clay retain their morphology and integrity in bond points better than control PP after calendering. Under the same processing conditions, fibers with additives retained their structural integrity after thermal calendering. Similar results were observed in our earlier studies of spunbond trial with incorporation of organo modified clay (Closite 15A) and natural nanoclay (Closite Na^+).[3] SEM micrographs of spunbond web failure structure at bond point for control PP web and webs with 1 wt % clay are shown in Figure 10(c,d). Micrographs depict difference in failure mechanism between the web samples. Most of the failures in the case of control PP webs were due to fiber breakage at bond edge, whereas, the failure in case of spunbond webs with nanoclay additives were due to fiber pull off [Fig. 10(e)] from bond point [Fig. 10(d)]. Increased clay loading had adverse effect on

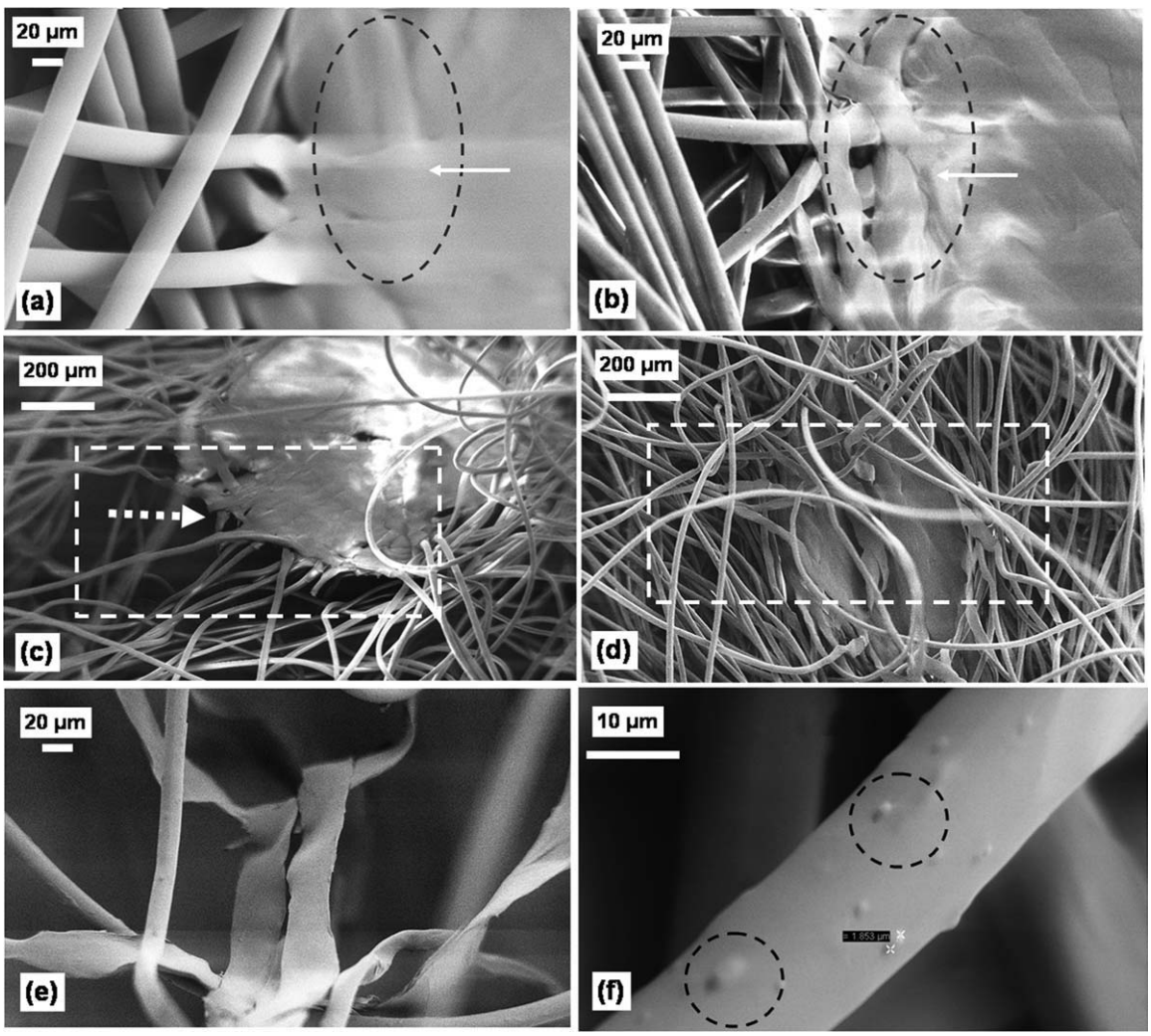

Figure 10 SEM micrograph of (a) bond point of control SB web, (b) bond point with 1% clay fibers retain their structure, (c) control SB bond failure point which indicates most of failure at bond edge, (d) failed bond point of web with 1% clay which is full of pulled off fibers, (e) pulled off fiber strip with 1% clay and (f) agglomerates on fiber surface with 2% clay.

the surface topology. SEM micrograph of fiber surface with 1 wt % clay is shown in Figure 10(f). The micrograph shows 0.5 to 1.76 μ particle on fiber surface of web sample with higher level of clay. These are due to nonuniform dispersion, and protrusion of tactoids from the surface. The protrusion of agglomerate clay stack from surface is also shown in TEM micrograph in Figure 7(a).

Statistical analysis showed significant decrease (student t test, $P << 0.05$) in the mechanical properties for sample with 2 and 5 wt % clay additives. These mechanical property differences are due to change in polymer microstructure because of the presence of additives. To understand this difference, an investigation on spherulite microstructure was performed using polarized light microscope.

Spherulite microstructure

Spherulite micrograph's for different samples are shown in Figure 11. Incorporation of nanoclay additive significantly changes the microstructure. Spherulite micrograph's clearly show the nucleating effect. The number of spherulite per unit area, maximum attainable diameter D_m and nucleation density N is included in Supporting Information Figures S3(a–c). Although the concentrates were crystallized in static condition and results could not be directly related to spunbond process, the spherulite micrographs give clear representations of the difference in the morphology and change in polymer microstructure in the presence of additives.

With the increase in clay wt %, segregation and hence reinforcement in the interspherulitic region was observed as shown in Figure 11(b,c,d). This segregated mass may consist of compatibilizer maleated wax along with excluded clay agglomerate. The area of interspherulitic region was 377 μm^2 for control PP and 580 μm^2 for PP with 1 wt % clay, respectively.

To investigate the composition of interspherulite region, combination of EDS and SEM was used.

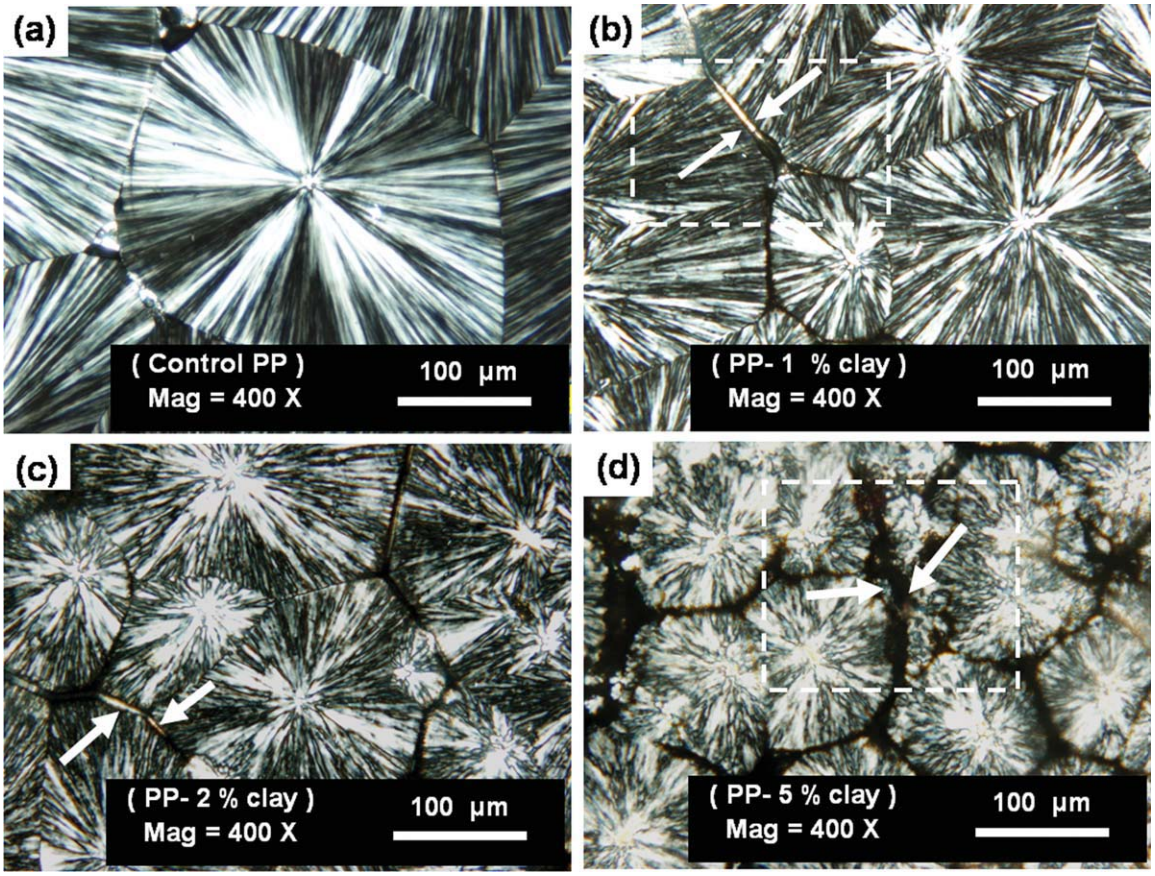

Figure 11 Polarized light micrographs of (a) control PP (b) PP with 1 wt % clay (1% clay + 5 % maleated wax + 94% PP) (c) PP with 2 wt % clay (d) PP with 5 wt % clay. [Color figure can be viewed in the online issue, which is available at www.interscience.wiley.com.]

SEM micrograph of interspherulitic region and EDS scan of sample with 1% clay are shown in Figure 12. EDS scans revealed clay chemistry in the interspherulite regions. The segregation at the interspherulitic region is due to the exclusion of clay platelets from the growing boundaries of the spherulites. The mechanism of clay exclusion from the PP chains is similar to zone refining.[34] During the solidification, the un-included clay platelets from the agglomerated mass are excluded out of crystal boundary. The results of reinforcement in the interspherulite region observed from the SEM and EDS results further elucidate the reason for slight improvement in dimensional stability results shown in Figure 9(b,c).

Discussion

Sample with 5 wt % clay in maleated PP matrix could not be processed due to rise in pressure. At low shear rates, shear viscosity increased for all the concentrates. This increase in viscosity is due to the agglomeration, entanglement of polymer chains and clay platelets. The entanglements between nanoclay additives and the polymer chains resist the free motion of melt and increase melt viscosity. TEM micrographs revealed mixtures of intercalated and exfoliated morphology for all the nanocomposite webs (Figures 5, 6, and 7). The nature of dispersion and clay stack morphology observed in the concentrates (Fig. 4) was also present in the SB webs. This demonstrates the need for better dispersion in the concentrates to get higher dispersion in the fiber based nanocomposite end products.

From the spherulite microstructure analysis, it is clear that, with increase in clay add on level, the number of spherulites per unit area increases and impurity rich spherulite boundaries are formed by exclusion of clay platelets at spherulite boundary. At higher weight percentage, because of large variation in distribution of sizes, there is increase in overall weak spots in a given unit area. Having these large variations in size distribution prevents efficient load transfer between matrix and filler platelets.

The MD tensile properties did not show any improvements even at low weight percentage add on level because of inefficient load transfer between platelet and matrix. Difference in failure mode and preservation of fiber integrity in bond point of SB

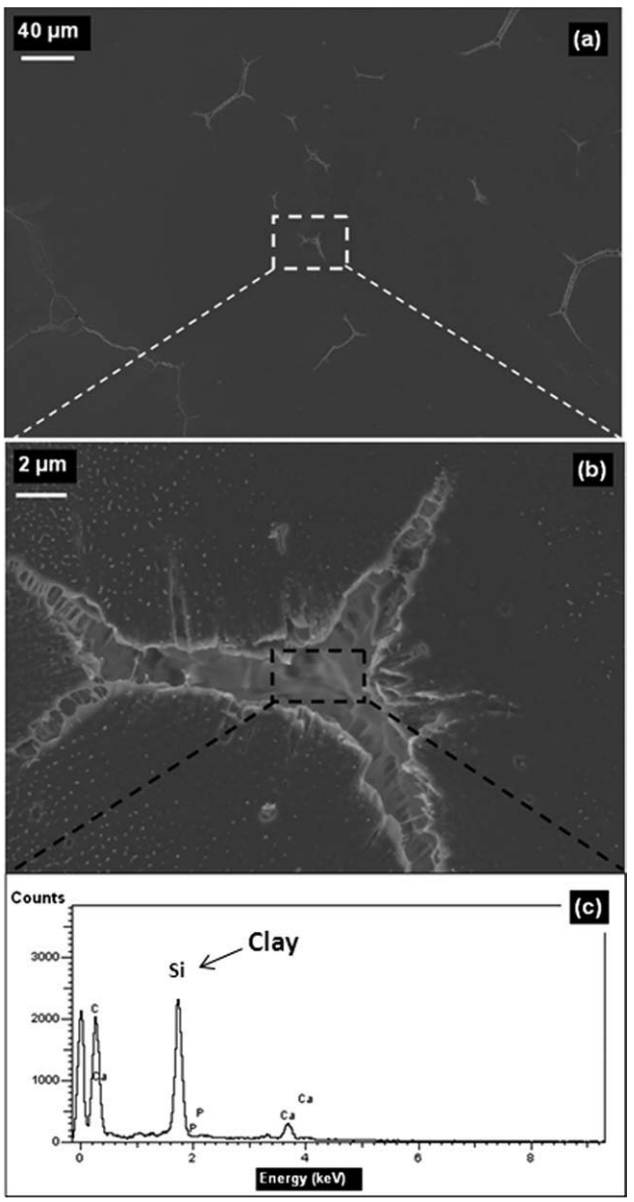

Figure 12 (d) SEM micrograph of interspherulitic region on a spherulite of PP with 1 wt % clay, (e) SEM micrograph at higher magnification, (f) EDS of interspherulitic region of PP with 1 wt % clay.

webs with additives might be due to the change in microstructure and toughening of ingredient fibers with additive.

Two different effects might be involved during extrusion of polymer melt with additives. First, cooling rate and kinematics are totally different due to presence of additives, and webs with additives cool at faster rate.[35] Since the fibers are cooled faster, the extent of stress induced orientation might be different in the case of fibers with additives. Birefringence results (shown in Table IV) did not show any significant difference. Second, clay additives act as nucleating agents, increase the crystallization kinetics and fiber crystallinity.[13,36] However, thermal analysis of fibers showed lower crystallinity wt % for all sample with additives.

Hence, increase in nonwoven web stiffness is due to the reinforcement effect of high modulus clay stacks (ranging from 20 to 400 GPa[32]) in matrix and exclusion of excess clay platelets in the interspherulite regions. The reinforcement in the amorphous region makes the molecular network more compact and restricts the motion of molecules.

CONCLUSIONS

The nanocomposite morphology, microstructure, and mechanical properties of nanoclay incorporated polypropylene webs are discussed here. Overall, nanoclay affects SB processing to a limited extent up to 2 wt % loading and at 5 wt % leads to processing difficulties. Concentrate with 5 wt % nanoclay in maleated polypropylene could not be processed because of the rise in viscosity. In case of polypropylene concentrates, TEM micrographs revealed good dispersion of additives for sample with up to 2 wt % of clay. Intercalated and flocculated morphology was observed for all the concentrates and the same morphology also subsists in SB webs. Size of tactoids increased for samples with 5 wt % additive. About 25 to 30% increase in CD direction tear strengths were observed for 1 to 2 wt % clay loading. Failure mechanism was different for spunbond fabrics with additives. Webs with even as low as 1 wt % clay retain their morphology and integrity in bond point after thermal bonding. The webs with additives showed lower shrinkage compared with that of control polypropylene webs. At higher weight percentage, stiffness of webs significantly increased and tear strength of webs decreased which may be due to exclusion of excess clay platelets in the interspherulite regions.

References

1. Alexandre, M.; Dubois, P. Mater Sci Eng 2000, 28.
2. Mlynarcikova, Z.; Kaempfer, D.; Thomann, R.; Mulhaupt, R.; Borsig, E.; Marcincin, A. Polym Adv Technol 2005, 16, 362.
3. Bhat, G. S.; Hegde, R. R.; Kamath, M. G.; Deshpande, B. J Eng Fibers Fabrics 2008, 3, 3.
4. Hussain, F.; Hojjati, M.; Okamoto, M.; Russell, G. E. J Compos Mater 2006, 40, 1511.
5. Tjong, S. C. Mater Sci Eng 2006, 53, 73.
6. Dasari, A.; Yu, Z.; Wing, Y.; Hua, G.; Joël, V. Compos Sci Technol 2005, 65, 2314.
7. Liu, X.; Wu, Q. Polymer 2001, 42, 10013.
8. Hasegawa, N.; Okamoto, H.; Kawasumi, M.; Kato, M.; Tsukigase, A.; Usuki, A. Macromol Mater Eng 2000, 280, 76.
9. Nam, P. H.; Maiti, P.; Okamoto, M.; Kotaka, T.; Hasegawa, N.; Usuki., A. Polymer 2001, 42, 9639.
10. Joshi, M.; Viswanathan, V. J Appl Polym Sci 2006, 102, 2164.
11. Rogers, K.; Takacs, E.; Thompson, M. R. Polym Test 2005, 24, 423.

12. Zhang, J.; Jiang, D. D.; Wilkie, C. A. Thermochim Acta 2005, 430, 107.
13. Kim, B.; Lee, S. H.; Lee, D.; Ha, B.; Park, J.; Char, K. Ind Eng Chem Res 2004, 43, 6082.
14. Opalko, R. J. Evaluation of the effects of nanofil nanoclays in the blending of polypropylene and polystyrene, Thesis, Akron, OH, 2008.
15. Jeziórska, R. Pigment Resin Technol 2006, 35, 3.
16. Bettini, S. H. P.; Agnelli, J. A. M. Polym Test 2000, 19, 3.
17. Chow, W. S.; Mohd Ishak, Z. A.; Karger-Kocsis, J.; Apostolov, A. A.; Ishiaku, U. S. Polymer 2003, 44, 7427.
18. Malkan, S. R.; Wadsworth, L. C. INB Nonwovens 1992, 3 (Part I), 4.
19. Shah, R. K.; Paul, D. R. Polymer 2006, 47, 4075.
20. Bhat, G. S.; Hegde, R. R.; Gulgunji, P.; Vempati, R. Nonwoven Tech Text 2007, 1, 23.
21. Malkan, S. R.; Wadsworth, L. C. Nonwovens 1992, 4, 24.
22. Hegde, R. R. Thermal bonding of polypropylene films and fibers, J Appl Polym Sci 2008, 110, 3047–3058.
23. Cullity, B. D.; Stock, S. R. Elements of X-Ray Diffraction, 3rd ed; Prentice Hall: New Jersey, USA 2001; 556–557.
24. METTLER TOLEDO. METTLER TOLEDO DSC 822e STARe Software user manual DSC evaluations.
25. ASTM International. Standard Test Methods for Nonwoven fabrics. ASTM D1117-97, ASTM International 2003.
26. Maiti, P.; Nam, P. H.; Okamoto, M.; Hasegawa, N.; Usuki, A. Macromolecules 2002, 35, 2042.
27. Hatzikiriakos, S. G.; Rathod, N.; Muliawan., E. B. Polym Eng Sci 2005, 45, 1098.
28. Krishnamoorti, R.; Vaia, R. A.; Giannelis, E. P. Chem Mater 1996, 8, 1728.
29. Fornes, T. D.; Yoon, P. J.; Keskkula, H.; Paul, D. R. Polymer 2001, 42, 25.
30. Sinha Ray, S.; Okamoto, M. Prog Polym Sci 2003, 28, 1539.
31. Svoboda, P.; Zeng, P.; Wang, H.; James, L.; David, L.; Tomasko, L. J Appl Polym Sci 2002, 85, 1562.
32. Levent, A.; Altan, M. C. Polym Compos 2009, 9999.
33. Trznadel, M.; Kryszewski, M. J Macromol Sci 1992, 32, 259.
34. Mullin, J. W. Crystallization, 4th ed; Butterworth-Heinemann: Oxford, UK, 2001.
35. Amish, L. M. In Benefits of Inorganic Additives in Meltblown Polypropylene; INTC: Texas, 2008.
36. Yu, J.; He, J. Polymer 2000, 41, 3.
37. Barnes, H. A.; Hutton, J. F.; Walters, K. An Introduction to Rheology, 1st ed; Elsevier Science Publishers: Oxford, UK 1989.